Available online at www.sciencedirect.com
SCIENCE DIRECT®
ELSEVIER
International Journal of Mechanical Sciences 46 (2004) 81–98
International Journal of MECHANICAL SCIENCES
www.elsevier.com/locate/ijmecsci

# On fracture locus in the equivalent strain and stress triaxiality space

Yingbin Bao, Tomasz Wierzbicki*

*Impact and Crashworthiness Laboratory, Massachusetts Institute of Technology, 77 Massachusetts Avenue, Cambridge, MA 02139, USA*

Received 2 July 2002; received in revised form 3 February 2004; accepted 4 February 2004

**Abstract**

The stress triaxiality is, besides the strain intensity, the most important factor that controls initiation of ductile fracture. In this study, a series of tests including upsetting tests, shear tests and tensile tests on 2024-T351 aluminum alloy providing clues to fracture ductility for a wide range of stress triaxiality was carried out. Numerical simulations of each test was performed using commercial finite element code ABAQUS. Good correlation of experiments and numerical simulations was achieved. Based on the experimental and numerical results, the relation between the equivalent strain to fracture versus the stress triaxiality was quantified and it was shown that there are three distinct branches of this function with possible slope discontinuities in the transition regime. For negative stress triaxialities, fracture is governed by shear mode. For large triaxialities void growth is the dominant failure mode, while at low stress triaxialities between above two regimes, fracture may develop as a combination of shear and void growth modes.
© 2004 Elsevier Ltd. All rights reserved.

*Keywords:* Fracture; Stress triaxiality; Experiment; Numerical simulation

## 1. Introduction

McClintock [1] and Rice and Tracey [2] have shown that fracture of ductile metals are strongly dependent on hydrostatic stress by studying growth of long cylindrical voids and spherical voids, respectively. Atkins [3,4] also pointed out that the criteria for fracture initiation should dependent on hydrostatic stress. This conclusion has been independently arrived at by empirical routes [5–7],

* Corresponding author. Tel.: 1-617-253-2104; fax: 1-617-253-8125.
*E-mail address:* wierz@mit.edu (T. Wierzbicki).

0020-7403/$ - see front matter © 2004 Elsevier Ltd. All rights reserved.
doi:10.1016/j.ijmecsci.2004.02.006

**Nomenclature**

| | |
|---|---|
| $\sigma_H$ | hydrostatic stress |
| $\bar{\sigma}$ | equivalent stress |
| $\sigma_H/\bar{\sigma}$ | stress triaxiality |
| $r$ | the radius of the minimum cross-section |
| $R$ | the radius of the circumferential notch |
| $R_0$ | the initial value of $R$ |
| $\bar{\varepsilon}$ | equivalent strain |
| $\bar{\varepsilon}_f$ | equivalent strain to fracture |
| $u$ | displacement |
| $u_f$ | displacement to fracture |
| $D/H$ | ratio of initial diameter to initial height of upsetting tests |
| $\mu$ | friction coefficient |
| $(\sigma_H/\bar{\sigma})_{av}$ | average stress triaxiality |

by porous plasticity or void growth mechanics modeling [1,2,8,9], by continuum damage mechanics [10], and by connecting initiation and propagation toughness mechanics [11–14]. Bao and Wierzbicki [15] among others [16–19] have also observed that the mechanism of fracture is different depending on the amount of triaxiality.

Fracture ductility is understood as the ability of a material to accept large amount of deformation without fracture. Equivalent strain to fracture is a good measurement of fracture ductility. Studies of effect of stress triaxiality on fracture ductility for metals performed in the past were mainly restricted to high stress triaxiality regime by using pre-notched round tensile specimens and negative stress triaxialities by upsetting specimens. Hancock and Mackenzie [20] carried out a series of tensile tests on pre-notched steel specimens. They found that the ductility depends markedly on the triaxiality of the stress state. The results of Bridgman's [21] approximate solution was applied in their study. The main features of Bridgman's [21] analysis are that equivalent strain is constant across the minimum cross section (numerical simulations have shown that there is variation of the equivalent strain along the cross section and the maximum equivalent strain occurs at the center of the specimen [15]), but the radial, hoop and axial stresses vary. The value of stress triaxiality increases from $\frac{1}{3}$ at the surface to a maximum value on the axis of the specimen, which is given by the famous Bridgman equations

$$\left(\frac{\sigma_H}{\bar{\sigma}}\right)_{\max} = \tfrac{1}{3} + \ln\left(\frac{r}{2R} + 1\right), \tag{1}$$

$$\bar{\varepsilon}_f = 2\ln\left(\frac{r_0}{r}\right), \tag{2}$$

where, $\sigma_H$ and $\bar{\sigma}$ are hydrostatic stress and equivalent stress, respectively, $\sigma_H = (\sigma_1 + \sigma_2 + \sigma_3)/3$, $\bar{\sigma} = \sqrt{1/2[(\sigma_1 - \sigma_2)^2 + (\sigma_2 - \sigma_3)^2 + (\sigma_3 - \sigma_1)^2}$, where $\sigma_1, \sigma_2$ and $\sigma_3$ are principal stresses; $r$ is the radius of the minimum cross-section and $R$ is the radius of the circumferential notch; $\bar{\varepsilon}_f$ is equivalent strain to fracture; $r_0$ is the initial value of $r$. Various authors correlated the experimental results with

the Rice–Tracey exponential function. Wierzbicki et al. [19] found that the following equation:

$$\bar{\varepsilon}_f = \left(\frac{\sigma_H}{\bar{\sigma}}\right)^n \tag{3}$$

with $n = -\frac{5}{3}$ gives a better correlation with Hancock's experimental data than the Rice-Tracey criterion. Recently, Mirza et al. [22] performed an experimental and numerical study on three different materials and obtained relations of $\bar{\varepsilon}_f$ and $\sigma_H/\bar{\sigma}$ for the high stress triaxiality. However, the literature still lacks studies of fracture ductility in the entire range of stress triaxialities.

Given the wealth of experimental data and good physical understanding of factors governing the onset of ductile fracture it is surprising that many leading nonlinear commercial codes such as ABAQUS, LS-DYNA and PAM-CRASH still use an overly simplified fracture criterion.

$$\bar{\varepsilon} = \bar{\varepsilon}_f \tag{4}$$

which is independent on stress triaxiality (Fig. 1 (a)). According to this approach fracture will occur equally well under tension and compression. The results of upsetting tests proved conclusively that there is a cut-off value $\sigma_H/\bar{\sigma} = -\frac{1}{3}$ below which fracture will never occur no matter what the magnitude of the equivalent strain may be, Fig. 1(b). For a plane stress condition the fracture zone in the $\bar{\varepsilon} - \sigma_H/\bar{\sigma}$ space can be mapped into the plane of principal stress or strain space. The regimes "forbidden" to fracture are shaded in Fig. 2.

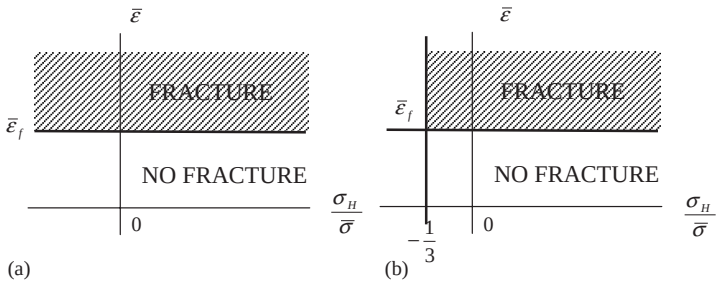


Fig. 1. Fracture criterion in leading commercial codes.

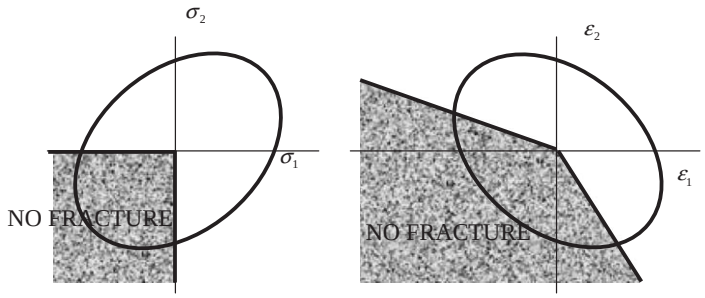


Fig. 2. Fracture zone in plane stress condition.

The presentation of the fracture criteria by two lines as shown in Fig. 1(b) is appealing but too simplistic for practical applications. The objective of the present research is to find the actual boundary between the fracture and no-fracture zone on the plane $\bar{\varepsilon}-\sigma_H/\bar{\sigma}$ (fracture locus) for a wide range of triaxialities. In this study, relations between $\bar{\varepsilon}_f$ and $\sigma_H/\bar{\sigma}$ were determined from different tests which cover a wide range of the stress triaxiality i.e. from $-\frac{1}{3}$ to 0.95. The limiting fracture curve for the range of negative stress triaxiality was obtained from compression tests. The relation for the range of low stress triaxiality was determined by a pure shear test, a test under combined shear and tensile loading and a test on a plate with a circular hole under tensile loading. Finally, the locus of fracture point in the range of high stress triaxiality was obtained by the classical tensile tests on notched specimens.

## 2. Approach

A limiting fracture curve was found by comparing experimental results with detailed numerical simulations. The procedure is briefly described as follows:

(1) Perform a series of tests and obtain force–displacement responses.
(2) Perform parallel numerical simulations.
(3) Determine from tests location of fracture initiation and displacement to fracture $u_f$ for each case.
(4) Calculate evolution of the equivalent strain and the stress triaxiality at the fracture location ($\bar{\varepsilon}$ vs. $u$ and $\sigma_H/\bar{\sigma}$ vs. $u$) for each case.
(5) Determine the equivalent strain to fracture and the average stress triaxiality for each case.
(6) Plot the results from Step 5 in $\bar{\varepsilon}-\sigma_H/\bar{\sigma}$ space and construct the limiting fracture curve.

## 3. Experiment

A series of 11 tests described in Table 1 including upsetting tests, shear tests and tensile tests on 2024-T351 aluminum alloy were performed to predict the dependence of fracture ductility in a wide range of the stress triaxiality. All the specimens were cut from a 6' long, 6" wide and 3" thick block of 2024-T351 aluminum alloy.

### 3.1. *Tests for negative stress triaxialities* (−0.3–0)

(a) *Conventional upsetting test*. One of the commonly used tests for fracture study is the uniaxial compression of short cylindrical specimens between flat platens (the so-called upsetting test). Because of friction between specimens and flat platens, a barreling effect occurs during the experiment near the equator. The resulting secondary circumferential tensile stresses are developed causing the specimen to fracture. Upsetting tests provide clues to the onset of fracture in the regime of negative stress triaxialities. In this study, compression tests were carried out on the cylinders shown in Fig. 3 with ratios of initial diameter to initial height $D/H$ 0.5, 0.8, 1.0 and 1.5. Deformed specimens are illustrated in Fig. 4. A strong barrel effect and the resulting 45° crack can be clearly seen. Identical specimens were compressed to different stages in order to capture the fracture initiation

Table 1
List of the tests

| Test number | Loading | Specimen description | Stress triaxiality $\sigma_H/\bar{\sigma}$ |
|---|---|---|---|
| 1 | Compression | Cylinder ($D/H = 0.5$) | $-0.33$ to $-0.12$ |
| 2 | Compression | Cylinder ($D/H = 0.8$) | $-0.32$ to $-0.05$ |
| 3 | Compression | Cylinder ($D/H = 1.0$) | $-0.32$ to $-0.05$ |
| 4 | Compression | Cylinder ($D/H = 1.5$) | $-0.32$ to $-0.05$ |
| 5 | Compression | Asymmetric (Fig. 6) | $-0.4$ to $-0.09$ |
| 6 | Shear | Flat (Fig. 8) | 0 to 0.02 |
| 7 | Combined shear and tension | Flat (Fig. 9) | 0.04 to 0.15 |
| 8 | Tension | Plate with a circular hole (Fig. 10) | 0.33 |
| 9 | Tension | Round, smooth | 0.33 to 0.5 |
| 10 | Tension | Round, large notch | 0.6 to 0.7 |
| 11 | Tension | Round, small notch | 0.9 to 1 |

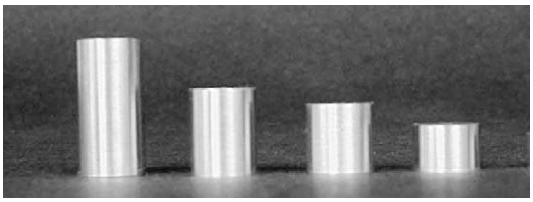

Fig. 3. Cylinders with different ratio of diameter and height.

Fig. 4. Deformed specimens with different ratios showing shear fracture.

more accurately. Fig. 5 shows representative specimens at different stages of compression. It was observed that fracture occurred in the equatorial area.

(b) *New compression test*. Conventional upsetting tests involve a certain amount of friction between specimens and flat platens. The presence of friction is responsible for the barrel effect and fracture, but it also brings difficulties and extra efforts in performing numerical simulations (see the numerical simulation section). A new promising type of compression test specimen shown in Fig. 6 was designed and performed, which removes the undesirable effect of friction and still

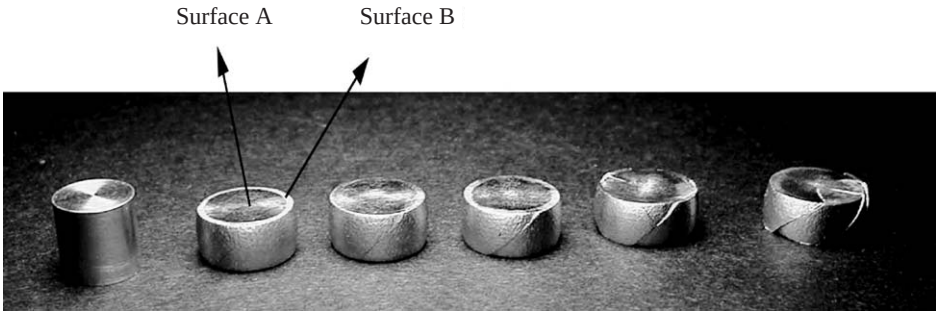


Fig. 5. Different stages of upsetting tests.


Fig. 6. A new configuration of compression test.

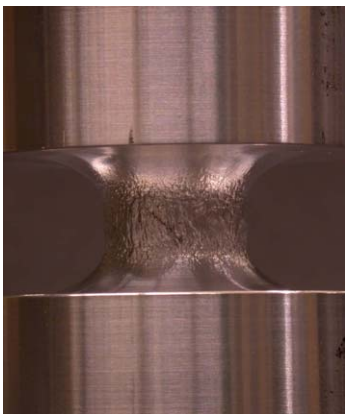

Fig. 7. Deformed specimens showing shear fracture.

provides fracture at the surface (Fig. 6). The specimen were machined as large diameter round bars with a notched small gauge section in the middle. The deformation is very localized in the gauge section and fracture initiation occurred at the equatorial area (Fig. 7). There is no deformation

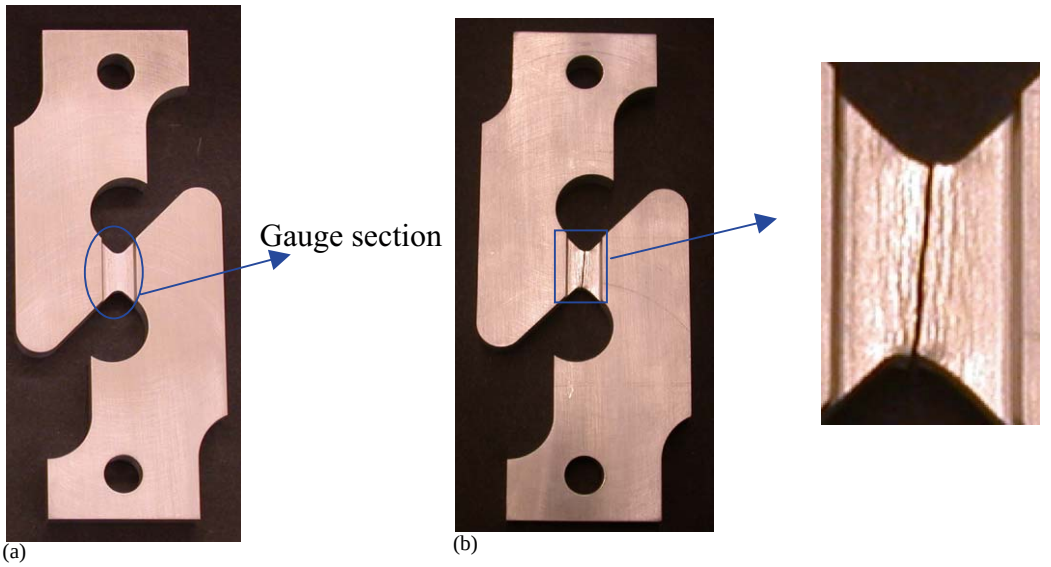


Fig. 8. A new specimen configuration of pure shear tests: (a) undeformed specimen and (b) fractured specimen.

in the shoulders and hence there is no horizontal force acting on the ends of the specimen due to friction. In other words, friction does not play a role in the test with this particular design.

### 3.2. *Tests for low stress triaxialities* (0–0.4)

A pure shear test, a test under combined loading (shear and tension) and a test on a plate with a circular hole under tensile loading were developed and carried out to get information of fracture ductility in the intermediate regime of the stress triaxiality.

(a) *Pure shear test*. A pure shear test is understood as one in which the hydrostatic pressure is zero or very small compared to the equivalent stress at fracture locations. In a search for the "best" shear test, a new specimen configuration shown in Fig. 8(a) was developed using the concept of a "butterfly" gauge section. The specimen was pulled through two pins. Fractured specimen is displayed in Fig. 8(b), from which it can be clearly seen that fracture occurred due to shear.

(b) *Test under combined loading*. By changing the shape of the gauge section of the pure shear test, a specimen configuration for combined shear and tension loading shown in Fig. 9(a) was developed. Fractured specimen is illustrated in Fig. 9(b), from which it can also be inferred that fracture occurs due to shear.

(c) *Test on plates with a circular hole under tensile loading*. A number of tests were preformed on flat rectangular bars with a circular hole subjected to tensile load [23]. As an example, Fig. 10 shows the initial and final shape of one of the specimens (4 mm thick, 50 mm wide and 20 mm radius of the hole). Fracture initiated at the middle of the circumferential surface of the cut-out perpendicular to the load. This test gives a stress triaxiality $\sigma_H/\bar{\sigma} = 0.33$ at the critical location [23].

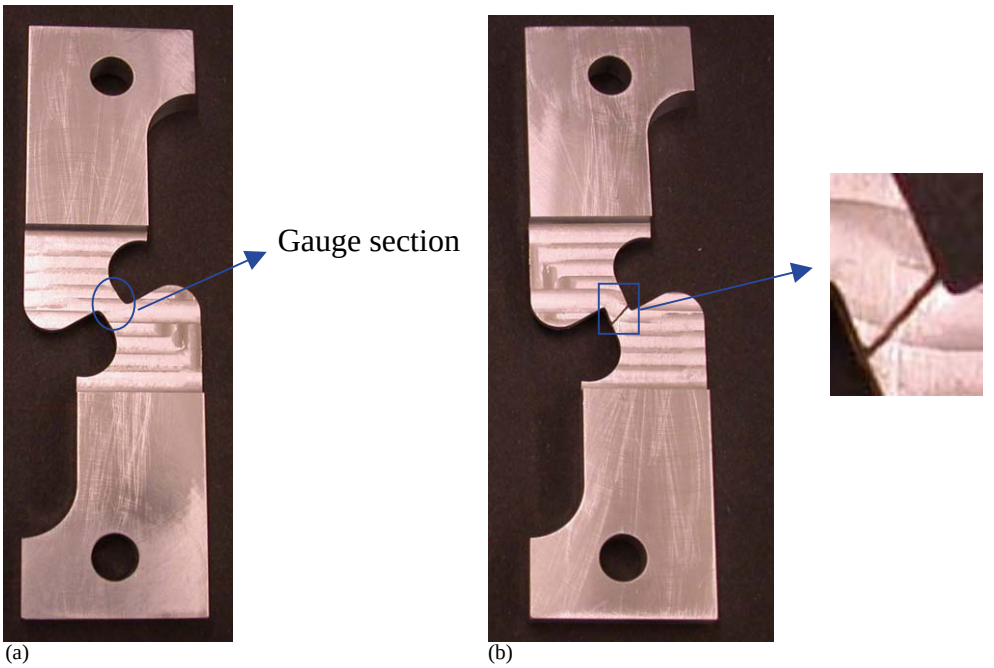


Fig. 9. A new specimen configuration of tests under combined loadings: (a) undeformed and (b) fractured.

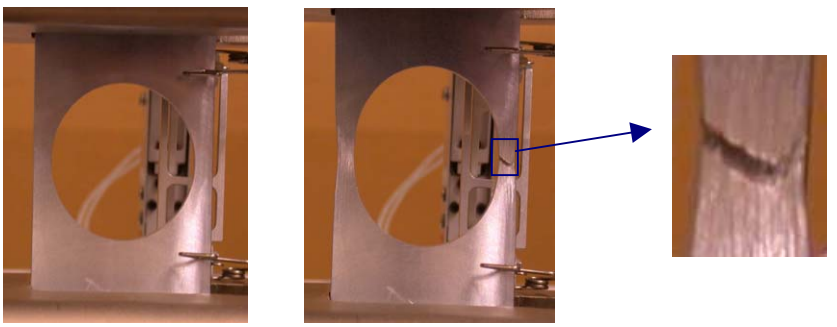

Fig. 10. Initial and final deformed shapes.

### 3.3. *Tests for high stress triaxialities* (0.4–0.95)

Conventional tensile tests were carried out on smooth round specimens and also on specimens with two different circumferential notches. Fracture initiated at center of the bar, where the stress triaxiality and equivalent strain were the largest [15,20]. Those tests give information of fracture ductility for the range of high stress triaxialities (0.4–0.95). The fractured specimens are illustrated in Fig. 11.

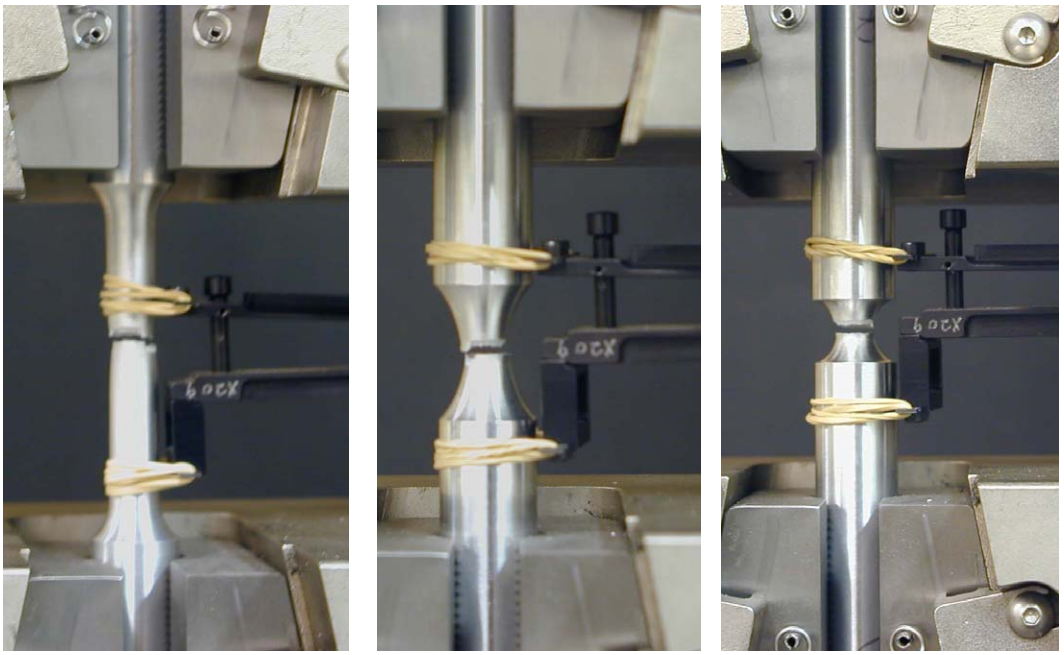

(a) (b) (c)

Fig. 11. Fractured tensile specimens. The specimens have the same diameter (9 mm) of the minimum cross section): (a) smooth; (b) $R = 12$ mm and (c) $R = 4$ mm.

## 4. Numerical simulation

Parallel numerical simulations of all the tests were carried out using commercial finite element code ABAQUS in order to obtain individual components of stress and strain tensors at fracture locations. Four-node axisymmetrical elements, shell elements or solid element were introduced. A detailed description on the way of determining the true stress–strain curve of the material was described in Ref. [15]. For the completeness of the present paper, this curve for both tension and compression is shown in Fig. 12. As a material model, we chose the isotropic plastic model (J2 plasticity) from the material input data in ABAQUS.

As an example, the deformed shape for the pure shear test is shown in Fig. 13. The deformation is very localized in the gauge section. Correlation of the load–displacement response between the experiments and numerical simulations are almost perfect for all the cases. As an example the degree of the correlation for the upsetting tests and the new compression test is shown, respectively, in Figs. 14 and 15.

In the finite element model of conventional upsetting tests and the new compression test, cylindrical specimens were modeled as 4-node axisymmetrical elements. The compression platens were modeled as rigid surfaces. A surface-to-surface contact with friction was introduced to model the interaction between the platen and the specimen. A downward velocity boundary condition was applied at the top platen while the bottom platen was fixed. For conventional upsetting tests, friction coefficients between the platen and the specimen were determined by fitting the experimental and numerical

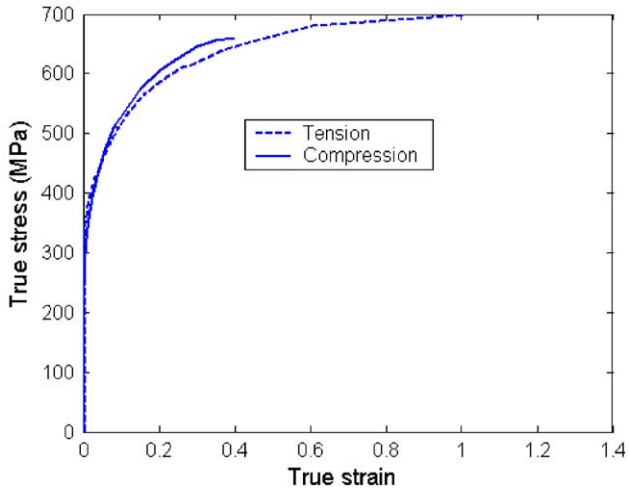


Fig. 12. True stress–strain curve for Al 2023-T351.

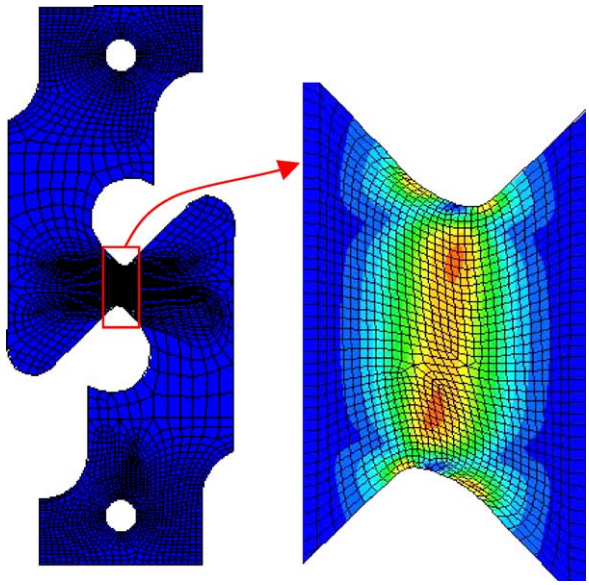

Fig. 13. Deformed shape of pure shear test specimen.

results. From the upsetting specimens depicted in Fig. 5, it can be found that the roughness of surface A and surface B (outer ring), which originally is part of the circumferential surface, is different. Therefore, different friction coefficients were used to model the friction between platen and surface A and the friction between platen and surface B in numerical simulations. Numerical simulations with different combinations of friction coefficients of platen-surface A and platen-surface B (see Fig. 3) were performed. The one with friction coefficient $\mu = 0.15$ for platen-surface A and $\mu = 0.5$ for platen-surface B gives good results (Fig. 14). Three friction coefficients 0, 0.2 and 0.5

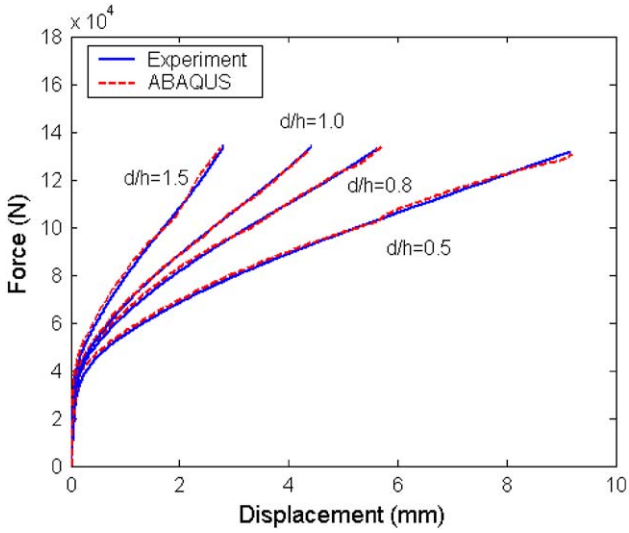


Fig. 14. Comparison of load-displacement response (conventional upsetting tests).

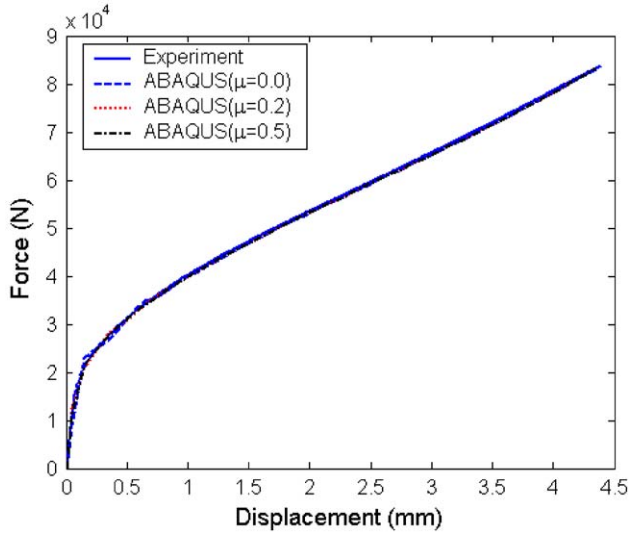


Fig. 15. Comparison of load–displacement response (new compression test).

were introduced in the new compression test to validate that there is no friction effect. Comparison of force–displacement response is displayed in Fig. 15. The correlation between experiment and numerical simulations are perfect. In addition, it is clearly shown that finite element models with different friction coefficients give the same result. Therefore, this test is indeed independent of the friction condition.

Eight-node solid elements were introduced to model the plate with a circular cut-out. A finite velocity was applied to one end of the model while the other end was fixed. For the pure shear, and combined shear and tension tests, shell elements were introduced. Two pins were modeled as rigid surfaces and a node-surface contact was introduced to model the interaction between the pin and the specimen. An upward velocity boundary condition was applied at one pin while another one was fixed. Plastic deformation is highly localized in the "butterfly" section.

Finally, numerical simulations of tensile tests on specimens with notch and without notch were also performed using ABAQUS. Four-node axisymmetrical elements were used to model the round specimens. A finite velocity was applied to one end of the model while the other end was fixed. The final diameter of the minimum cross section obtained from experiments and numerical simulations is very close.

## 5. Result

Since the correlation of the experimental and numerical results is almost perfect in terms of the load-displacement relation for all the cases considered in this study, it is reasonable to study the fracture ductility based on the individual components of stress and strain tensors at locations of fracture initiation obtained from numerical simulations.

From tests, fracture initiation is almost unequally defined at the critical locations by the displacement to fracture $u_f$. The critical locations of fracture onset were determined from experimental observation and numerical simulations. In the classical compression tests and tensile tests, critical locations were at the equatorial area and the center of the round bar, respectively. This observation was also reported by a number of other studies. It was clearly observed that fracture initiated at the middle of the circumferential surface of the hole perpendicular to the loading during the present experiments on plates with circular holes. It was not possible to capture the exact location of fracture initiation for the pure shear and the combined shear and tension during the tests. The critical location was determined as the one where the maximum equivalent strain is the highest along the path of the final crack obtained from the test.

The displacement to fracture was determined by both observations during experiments and the force–displacement responses. There is a significant load drop in the force–displacement responses in all tensile and shear tests. This drop is taken as the point of fracture initiation in this study. It is true that load could still increase even if structure starts to crack because of material hardening. However, it was observed that crack grows very rapidly during the tests. Therefore, it is reasonable to take the beginning of the drop as an approximate indication of the onset of fracture since those two stages are very close to each other. This type of sudden drop in force level did not occur in some of the upsetting tests. Therefore, fracture onset for upsetting tests was determined by observing the crack initiation on the external surface of the equatorial area during the experiment. Specimens of the upsetting tests were compressed to different stages and then were examined to determine exact stage of fracture initiation.

The numerical simulations provide exact values of stress and strain components and also load-displacement responses. The relationship between displacement and equivalent strain at the critical location can be obtained from the numerical simulation for each case. Then, the equivalent strain to fracture was determined as the equivalent strain which corresponds to the displacement to fracture $u_f$.

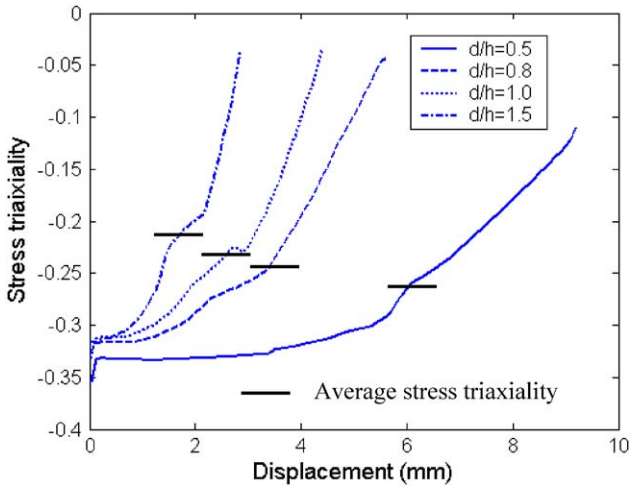


Fig. 16. Evolution of stress triaxiality for upsetting tests.

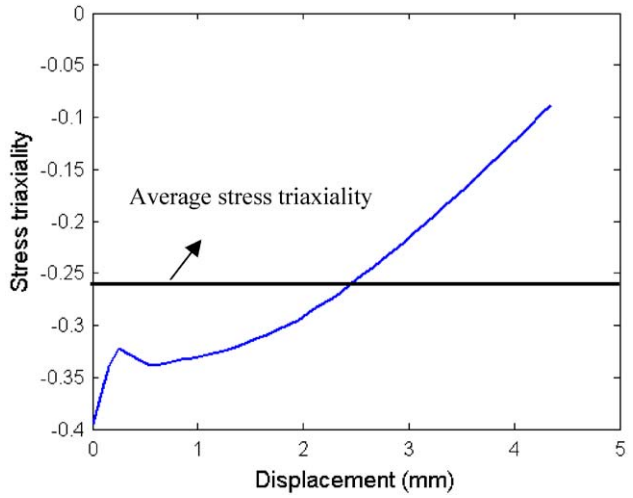


Fig. 17. Evolution of stress triaxiality for new compression tests.

Generally, the stress triaxiality during the entire deformation is not constant, especially in upsetting tests, the stress triaxiality changes significantly (Figs. 16–19). In order to construct the fracture locus in the $\bar{\varepsilon} - \sigma_H/\bar{\sigma}$ space, an average stress triaxiality is introduced, defined by

$$\left(\frac{\sigma_H}{\bar{\sigma}}\right)_{av} = \frac{1}{\bar{\varepsilon}_f}\int_0^{\bar{\varepsilon}_f} \frac{\sigma_H}{\bar{\sigma}}\, d\bar{\varepsilon}, \tag{5}$$

where $\bar{\varepsilon}$ is the equivalent strain and $\bar{\varepsilon}_f$ is the equivalent strain to fracture. The justification of the above averaging procedure comes from considering the fracture locus corresponding to high stress triaxiality. It was shown in Ref. [15] that onset of fracture in this range is controlled by the following

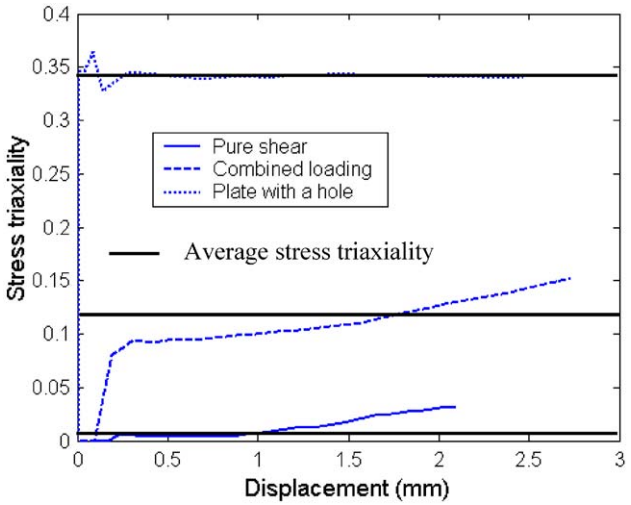


Fig. 18. Evolution of stress triaxiality for the tests in the range of medium stress triaxiality.

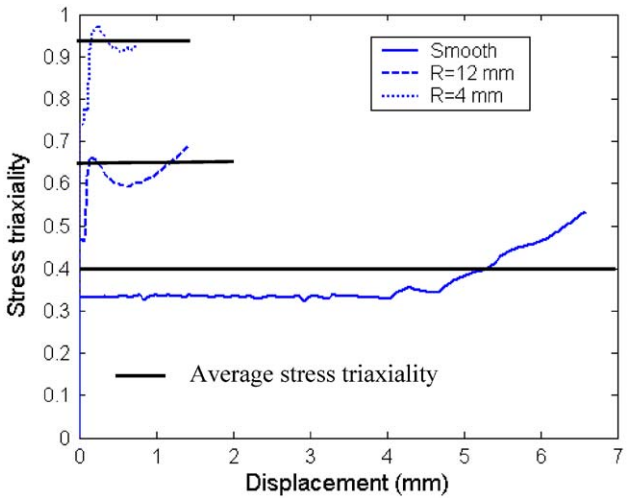


Fig. 19. Evolution of stress triaxiality for tensile tests.

functional reaching a critical value.

$$D = \int_0^{\bar{\varepsilon}_f} \frac{\sigma_H}{\bar{\sigma}}\, d\bar{\varepsilon} = \left(\frac{\sigma_H}{\bar{\sigma}}\right)_{av} \bar{\varepsilon}_f. \tag{6}$$

It can be seen that Eq. (5) is in fact a reinstatement of Eq. (6).

After obtaining the equivalent strain to fracture and the average stress triaxiality for each case, the fracture locus in $\bar{\varepsilon} - \sigma_H/\bar{\sigma}$ space was constructed shown in Fig. 20. It can be clearly seen that equivalent strain to fracture differs quite large for specimens under different stress triaxialities. In the range of negative stress triaixiality, the equivalent strain to fracture decreases with the stress

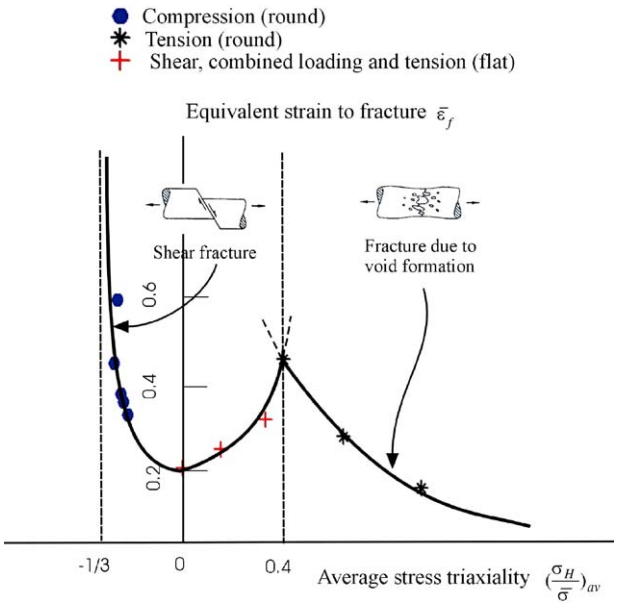


Fig. 20. Dependence of the equivalent strain to fracture on the stress triaxiality.

triaxaility and reaches a minimum of 0.2 at the stress triaxiality $\sigma_H/\bar{\sigma} = 0$, which corresponds to the pure shear test. Then it increases in the range of low stress triaxiality with the stress triaxiality and reaches a peak of 0.45 at the average stress triaxiality $\sigma_H/\bar{\sigma} = 0.4$ which corresponds to the tensile test on the smooth round bar. Finally, it decreases with the stress triaxiality in the range of high stress triaxiality.

## 6. Discussion

Shear fracture dominates in the upsetting tests, which is in the range of negative stress triaxialities. Fracture occurs due to void formation in tensile tests on pre-notched specimens which is in the range of high stress triaxialities, while at stress triaxialities between above two regimes, fracture may develop as a combination of shear and void growth modes. Still it is not quite clear how does the transition occur from the shear dominated fracture to fracture due to void formation. In this present paper, it would appear that the transition point from the shear dominated fracture to fracture due to void growth occurs around $\sigma_H/\bar{\sigma} = \frac{1}{3}$, corresponding to the tensile test on smooth round specimens.

In fact in the cup-and-cone failure, fracture initiation first at the center due to the void growth mode and then changes to shear fracture as the crack approaches the surface [24]. A change of the mechanism of fracture provides a clear slope discontinuity in the fracture locus, presented in Fig. 20. The transition from one mode to the other depends on the type of materials and for Al 2024-T351 it occurs at $\sigma_H/\bar{\sigma} = 0.4$.

There are a sufficient number of points on Fig. 20 to be able to develop an analytical representation of the fracture locus. It is convenient to distinguish three regimes and in each of these regimes

develop a simple analytical expression. In the case of negative triaxialities a suitable class of functions with a vertical asymptote was developed by Wierzbicki and Werner [25] based on experimental results of Kudo and Aoi [26]. Using this expression, the best fit of the present experiments on upsetting was obtained by the following expression:

$$\bar{\varepsilon}_f = 0.1225 * \left(\frac{\sigma_H}{\bar{\sigma}} + \frac{1}{3}\right)^{-0.46} \quad \text{for } \sigma_H/\bar{\sigma} = -1/3\text{–}0. \tag{7}$$

For low triaxialities (0–0.4) and for high triaxialities (0.4–0.95), a simple parabolic fit found to be satisfactory. The expressions are given in Eqs. (8) and (9), respectively.

$$\bar{\varepsilon}_f = 1.9 * \left(\frac{\sigma_H}{\bar{\sigma}}\right)^2 - 0.18 * \left(\frac{\sigma_H}{\bar{\sigma}}\right) + 0.21 \quad \text{for } \sigma_H/\bar{\sigma} = 0\text{–}0.4, \tag{8}$$

$$\bar{\varepsilon}_f = 0.15 \left(\frac{\sigma_H}{\bar{\sigma}}\right)^{-1} \quad \text{for } \sigma_H/\bar{\sigma} = 0.4\text{–}0.95. \tag{9}$$

A plot of the above three equations together with the experimental results is shown in Fig. 21. One can see that Eq. (9) is identical to Eq. (6) where the calibration constant $D_c = 0.15$. Note that the subscript "*av*" has been dropped in the above three equations.

The critical strain to fracture for the new compression tests were somewhat higher than the conventional upsetting tests on cylinders for the same amount of triaxialites. The discrepancy of the results obtained from these two types of upsetting tests should be explained in the future study. It would appear though that in the new compression specimen, the gauge section developed considerable amount of orange skin deformation. Therefore it was very difficult to observe visually the true onset of fracture.

It is recognized that the fracture locus is specific for a given material. The main contribution of the present paper is not necessary to derive such a locus for a particular aluminum alloy but rather to develop a general methodology for constructing the fracture locus for any ductile material. Besides

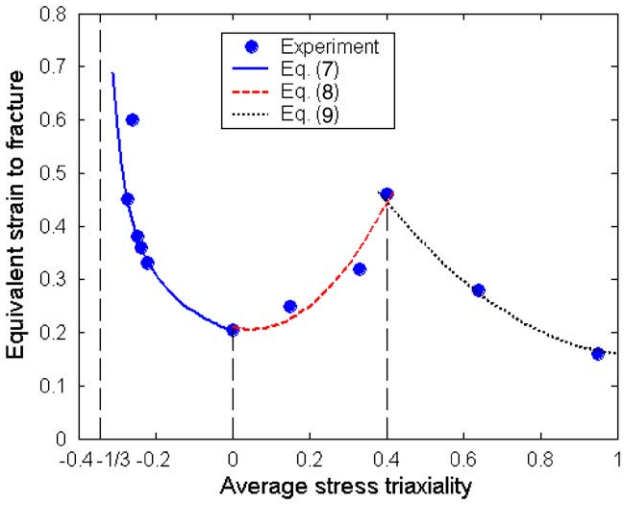


Fig. 21. Experiments vs. curve fitting.

the stress triaxiality, some other parameters may have some effect on fracture ductility such as plate thickness, stress and strain gradient etc. This issue is the subject of the subsequent study [23].

## 7. Conclusion

A series of tests including upsetting tests, shear tests, and tensile tests on 2024-T351 aluminum alloy, which provide clues to the dependence of fracture ductility on the stress triaxiality in a wide rage of this parameter, were carried out. Parallel numerical simulations of all the tests were performed using commercial finite element code ABAQUS. The correlation of experimental and numerical results in terms of the load–displacement relation is very good.

In this work, the fracture ductility was found strongly dependent on the stress triaxiality. It was also observed that shear fracture dominates in the upsetting tests which is in the range of negative stress triaxialities. Fracture occurs due to void formation in tensile tests on pre-notched specimens which is in the range of high stress triaxialities, while at low stress triaxialities between above two regimes, fracture may develop as a combination of shear and void growth modes. Based on these results the calibration procedure was developed and fracture locus was constructed in the space of the equivalent strain to fracture and stress triaxiality, suitable for practical applications. The main conclusion drawn from the present study is that there is a possible slope discontinuity in the fracture locus corresponding to the point of fracture mode transition.

## Acknowledgements

The present research was supported by the joint MIT/Industry Consortium on the Ultralight Metal Body Structure and the Volpe Center Grant to MIT.

## References

[1] McClintock FA. A criterion of ductile fracture by the growth of holes. Journal of Applied Mechanics 1968;35: 363–71.
[2] Rice JR, Tracey DM. On the ductile enlargement of voids in triaxial stress fields. Journal of the Mechanics and Physics of Solids 1969;17:201–17.
[3] Atkins AG. Fracture in forming. Journal of Materials Processing Technology 1996;56:609–18.
[4] Atkins AG. Fracture mechanics and metalforming: damage mechanics and the local approach of yesterday and today. In: Rossmanith HP, editor. Fracture Research in Retrospect, An Anniversary Volume in Honour of George R. Irwin's 90th Birthday. Rotterdam, Brookfield: A.A. Balkema; 1997. p. 327–52.
[5] Brozo P, Deluca B, Rendina R. A new method for the prediction of formability in metal sheet, sheet metal forming and formability. Proceedings of the 7th Biennial Conference of the IDDRG, Amsterdam, The Netherlands, 1972.
[6] Norris DM, Reaugh JE, Moran B, Quinones DF. A plastic-strain, mean-stress criterion for ductile fracture. Journal of Engineering Materials and Technology 1978;100:279–86.
[7] Oyane M, Sato T, Okimoto K, Shima S. Criteria for ductile fracture and their applications. Journal of Mechanical Work and Technology 1980;4:65–81.
[8] LeRoy G, Embury JD, Edward G, Ashby MF. A model of ductile fracture based on the nucleation and growth of voids. Acta Metallurgica 1981;29:1509–22.
[9] Sun J. Effect of stress triaxiality on micro-mechanisms of void coalescence and micro-fracture ductility of materials. Engineering Fracture Mechanics 1991;39:799–805.

[10] Rosa GL, Mirone G, Risitano A. Effect of stress triaxiality corrected plastic flow on ductile damage evolution in the framework of continuum damage mechanics. Engineering Fracture Mechanics 2001;68:417–34.
[11] Sun J, Deng Z, Tu M. Effect of stress triaxiality levels in crack tip regions on the characteristics of void growth and fracture criteria. Engineering Fracture Mechanics 1991;39:1051–60.
[12] Henry BS, Luxmoore AR. The stress triaxiality constraint and the Q-value as a ductile fracture parameter. Engineering Fracture Mechanics 1997;57:375–90.
[13] Ma H. The effect of stress triaxiality on the local cleavage fracture stress in a granular bainitic weld metal. International Journal of Fracture 1998;89:143–57.
[14] Atkins AG, Mai YW. Elastic and plastic fracture. Chichester: Ellis Horwood; 1988.
[15] Bao Y, Wierzbicki T. A comparive study on various ductile crack formation criteria. Journal of Engineering Materials and Technology, in press.
[16] Dieter GE. Workability testing techniques. American society for metals, Metals Park, Ohio, USA, 1984.
[17] Thomason PF. Ductile fracture of metals. Oxford: Pergamon Press; 1990.
[18] Hooputra H, Metzmacher G, Werner H. Fracture criteria for crashworthiness simulation of wrought aluminum alloy components, Proceedings of 11th Annual European Conference EuroPam, Heidelberg, Germany, 2001. p. 1–18.
[19] Wierzbicki T, Muragishi O. Calibration of ductile fracture from compression and tension tests. Impact & Crashworthiness Laboratory, Report No. 21, MIT, 1999.
[20] Hancock JW, Mackenzie AC. On the mechanisms of ductile failure in high-strength steels subjected to multi-axial stress-states. Journal of the Mechanics and Physics of Solids 1976;24:147–69.
[21] Bridgman PW. Studies in large plastic flow and fracture. Cambridge, MA: Harvard University Press; 1964.
[22] Mirza MS, Barton DC, Church P. The effect of stress triaxiality and strain-rate on the fracture characteristics of ductile metals. Journal of Materials Science 1996;31:453–61.
[23] Bao Y. Dependence of fracture ductility on thickness. Thin-Walled Structures, in press.
[24] McClintock FA, Argon AS. Mechanical behavior of materials. Reading, MA: Addison-Wesley Publishing Company, Inc.; 1965.
[25] Wierzbicki T, Werner H. Cockcroft and Latham Revisited. Impact & Crashworthiness Laboratory, Report No. 16, MIT, 1998.
[26] Kudo H, Aoi K. Effect of compression test conditions upon fracturing of medium carbon steel. Journal of Japanese Society of Technology and Plasticity 1967;8:17–27.